



ELSEVIER

Earth and Planetary Science Letters 203 (2002) 205–220

EPSL

www.elsevier.com/locate/epsl

Compaction in a mantle with a very small melt concentration: Implications for the generation of carbonatitic and carbonate-bearing high alkaline mafic melt impregnations

Michel Rabinowicz^a, Yanick Ricard^b, Michel Grégoire^{a,*}

^a *Laboratoire de Dynamique Terrestre et Planétaire, UMR 5562, Observatoire Midi-Pyrénées, 14, Avenue Edouard Belin, 31400 Toulouse, France*

^b *Laboratoire des Sciences de la Terre, Ecole Normale Supérieure, 46 allée d'Italie, 69364 Lyon, France*

Received 12 March 2002; accepted 12 July 2002

Abstract

Xenoliths entrained in alkaline basalts and kimberlites give strong evidence that mantle carbonatitic and carbonated high alkaline mafic silicate melts, which are initially produced at very low degrees of partial melting ($\ll 1\%$), percolate and accumulate to form impregnations with a melt concentration of up to 10%. At present no compaction model has explained such huge local amplification of melt concentration. Recently, Bercovici et al. [1] have shown that the commonly used equations of compaction are not sufficiently general to describe all melt percolation processes in the mantle. In particular, they show that, when the melt concentration in the mantle is very low, the pressure jump ΔP between the solid and liquid fractions of the mantle mush is very important and plays a driving role during compaction. 1-D compaction waves generated with two different systems of equations are computed. Three types of wave-trains are observed, i.e. (1) sinusoidal waves; (2) periodic waves with flat minima and very acute maxima ('witch hat waves'); (3) periodic solitary waves with flat maxima and extremely narrow minima ('bowler hat waves'). When the initial melt distribution in the mantle is quite homogeneous, the compaction waves have sinusoidal shapes and can locally amplify the melt concentration by a factor less than two. When there is a drastic obstruction at the top of the wetted domain, the pressure jump ΔP between solid and liquid controls the shape of the waves. If the computation assumes the equality of pressure between the two phases ($\Delta P = 0$), the compaction wave has a 'bowler hat shape', and locally amplifies the melt concentration by a factor less than 5. Alternatively, simulations taking into account the pressure jump between phases ΔP predict compaction waves with 'witch hat shape'. These waves collect a large quantity of melt promoting the development of magmons with local melt concentration exceeding $100\times$ the background melt concentration. It is inferred that in a mantle with very low concentrations of carbonatitic or high alkaline mafic silicate melt the magmons are about 1 km thick and reach, in less than 1 Ma, a melt concentration of about 10%. The magmons are likely generated below the lithosphere at some distance away from the center of hot spots. This can explain the development of mantle carbonatitic eruptions in the African rift and the carbonatite and high alkaline mafic silicate volcanic activity in oceanic islands.

© 2002 Elsevier Science B.V. All rights reserved.

* Corresponding author.

E-mail address: michel.gregoire@cnes.fr (M. Grégoire).

Keywords: melts; mantle; compaction; magmas; metasomatism; volcanism

1. Introduction

Petrological, mineralogical and geochemical studies of mantle xenoliths entrained in alkaline basalts and kimberlites give strong evidence that circulation of carbonatitic and carbonated high alkaline mafic silicate melts is well developed in the upper mantle [2–10]. These melts are commonly produced in the upper mantle at very low degrees of partial melting ϕ_0 ($\phi_0 \sim$ several 0.1%; [11–13]). Static experimental studies reveal low dihedral wetting angles of carbonate and high alkaline mafic silicate melts in contact with olivine (25–30°; [14,15]). It implies that films of fluid with a very small thickness (possibly as low as a few hundreds Å) wet the solid-grain boundaries and penetrate along the grain edges to form an interconnected network of melt tubes with roughly triangular cross sections [16]. Experiments performed to investigate the intercontinuity of carbonate melt in a dunite suggest that the mantle is permeable for any local melt concentration ϕ exceeding about 10^{-5} [17]. The melting rate of carbonatites ($\phi_0 \sim 0.1\%$) exceeds by two orders of magnitude the 10^{-5} permeability threshold. Also, because of the microscopic thickness of the inter-granular films (a few hundreds Å), these films likely still wrap the whole mantle grains when the local melt concentration ϕ is about 10^{-5} . Hence as soon as the melting process starts and as long as melt concentration ϕ is about 10^{-5} , both the wetting of the solid grain boundaries and the development of a tube network favor the percolation of the interstitial melt. These results illustrate the known unique capability of carbonatites and related melts to percolate within the upper mantle.

A power law relationship between permeability $k(\phi)$ and melt concentration ϕ is usually expected [18]:

$$k(\phi) \propto a^2 \phi^n \quad (1)$$

where n is a dimensionless constant and a designates

the characteristic size of the solid grains. When the melt flow is mainly confined in tubes along the grain boundaries, the power law constant n is ~ 2 , in case of a flow mainly confined in films, $n \sim 3$ [18]. Laboratory experiments suggest that mantle rocks with mm-size grains ($a \sim 1$ mm) and melt concentration $\phi \sim 0.01$ have permeabilities of $\sim 10^{-15}$ m² [19].

Because of the density difference $\delta\rho = \rho_m - \rho_f$ between the melt ρ_f and the solid ρ_m , the melt tends to flow upward while the solid compacts. During the mid-eighties, equations for mantle compaction were proposed [18,20,21]. A major goal of the modelings is to show that compaction induces melt impregnations. Barcillon and Richter [22] showed that an obstruction to the upward percolation of melt triggers transient compaction waves. The local melt concentration in these waves, called magmons, reaches several times the bulk melt concentration ϕ_0 . Melt impregnations below ridges or inside mantle hot spots can be associated with the development of magmons [23–26]. The models explaining the development of these magmons assume melts with a basaltic composition and an initial bulk concentration ϕ_0 exceeding several %. The bulk production of carbonatitic or alkaline mafic melts being extremely small, $\phi_0 \sim 0.1\%$, the magmons must amplify the local melt concentration ϕ by about two orders of magnitude to explain the 10% volume of melt locally found in some impregnations or the volume of melt erupted at some volcanoes [9,27]. At present no compaction process has been shown to provide such huge local amplification of melt concentration.

Recently, Bercovici et al. [1] discussed the assumptions necessary to derive the equations of compaction. Contrary to the interpretation of McKenzie [18] where the resistance of the matrix under isotropic stress is due to a bulk plastic viscosity, Bercovici et al. [1] attributes this resistance to the presence of a pressure jump between the solid and liquid phase P_m and P_f . This pressure jump $\Delta P = P_m - P_f$ is itself related to the rate of

porosity change:

$$\Delta P = -\frac{\mu_m}{\phi(1-\phi)} \frac{\overline{D}\phi}{Dt} \quad (2a)$$

where μ_m designates the mantle plastic viscosity and $\overline{D}\phi/Dt$ is the total derivative of ϕ . In:

$$\frac{\overline{D}\phi}{Dt} = \frac{\partial\phi}{\partial t}(\phi\mathbf{v}_f + (1-\phi)\mathbf{v}_m) + \overline{\nabla}\phi \quad (2B)$$

\mathbf{v}_m and \mathbf{v}_f designate the melt and solid velocities, and t is the time. Their interpretation implies that the bulk viscosity introduced by McKenzie should vary like μ_m/ϕ in agreement with the findings of other authors (e.g. Scott and Stevenson [23], Sumita et al. [28]). At last, Bercovici et al. [1] take into account the surface tension between phases that play a driving role in the development of compaction waves [29].

In the present paper, we reconsider the problem of modeling compaction waves using this new formalism. Our aim is to apply this subsequently to the percolation of carbonatitic and high alkaline mafic melts in the mantle. Because of the small melting rates ϕ_0 and low dihedral angles, the modeling assumes an infinitesimal melt concentration ϕ and a negligible surface tension between phases. In Section 3 we present the characteristics of some class of solitary waves solutions of the compaction equations. In Section 4 we show several transient, 1-D, numerical compaction experiments. In Section 5 we discuss conditions permitting the development of carbonatitic and high alkaline mafic melt impregnations in the mantle.

2. Mathematical formalism

In this section we first recall the basic equations, then we show how they are simplified and made dimensionless.

2.1. General equations

According to Bercovici et al.'s [1] formalism the

following equations must be used to model two phase flows.

2.1.1. Mass conservation of the melt

$$\frac{\partial\phi}{\partial t} + \overline{\nabla}(\phi\mathbf{v}_f) = 0 \quad (3a)$$

2.1.2. Mass conservation of the solid

$$\frac{\partial(1-\phi)}{\partial t} + \overline{\nabla}((1-\phi)\mathbf{v}_m) = 0 \quad (3b)$$

In Eqs. 3a and 3b, the density of both the fluid ρ_f and the solid ρ_m are assumed to be uniform. It is justified by the very small compressibility of the melt and of the solid in the mantle: a few times 10^{-11} Pa^{-1} [30].

2.1.3. The Darcy equation

This equation expresses the balance of stresses acting on the melt fraction ϕ of the porous media:

$$0 = \phi \left(-\overline{\nabla}(P_f + \rho_f g z) + \frac{\mu_f}{k(\phi)} \phi \Delta \mathbf{v} + \Delta P \overline{\nabla} \phi \right) \quad (3c)$$

Here $\Delta \mathbf{v} = \mathbf{v}_m - \mathbf{v}_f$, μ_f is the melt viscosity, g is the gravity acceleration and z is the height. In the above equation, the first term designates the pressure gradient, the second the viscous stress due to melt percolation and the last term the stress due to the pressure jump between the solid and the liquid ΔP .

2.1.4. The plastic flow equation

This equation controls the balance of stresses acting on the solid fraction $(1-\phi)$ of the porous media:

$$0 = -(1-\phi) \overline{\nabla}(P_m + \rho_m g z) + \overline{\nabla}((1-\phi)\tau_m) - \frac{\mu_f \phi^2}{k(\phi)} \Delta \mathbf{v} + (1-\phi) \Delta P \overline{\nabla} \phi \quad (3d)$$

The stress tensor in the solid fraction of the porous media is τ_m . From left to right, the different

terms of the equation correspond to: the effective pressure gradient in the solid; the viscous stress generated by the deformation of the solid; the stress due to the friction generated by the melt percolation and the stress due to the pressure step between the solid and the liquid. The elastic stresses resulting from the compressibility of both the melt and the solid phases are neglected here. Indeed, the elastic stresses are shown to play a role on compaction if either the fluid or the solid Deborah numbers exceeds one [31]. The Deborah number of the melt or of the solid is the product of its compressibility, here $\sim 10^{-11} \text{ Pa}^{-1}$, with the pressure contrast during compaction between melt and solid, here $< 3 \cdot 10^7 \text{ Pa}$ (Table 1). It results that, the Deborah numbers are very small, $< 10^{-3}$. We therefore do not take into account the elastic stresses in the equations.

2.1.5. Simplification of the equations

The equations are simplified according to the following statements. Let recall that:

$$\begin{aligned} \vec{\nabla}(1-\phi)\tau_m = \\ \vec{\nabla} \times (1-\phi)\mu_m \vec{\nabla} \times \mathbf{v}_m + \frac{4\mu_m}{3} \vec{\nabla}((1-\phi) \vec{\nabla} \mathbf{v}_m) \end{aligned} \quad (4a)$$

The first term of the right hand side corresponds

to stresses due to the shearing of the solid matrix and the last one to the stresses due to the compaction or the dilation of the solid matrix. In the following, we assume that the shearing stresses are negligible and thus we use the following simplified equation:

$$\vec{\nabla}(1-\phi)\tau_m = \vec{\nabla} \left((1-\phi) \frac{4\mu_m}{3} \vec{\nabla} \mathbf{v}_m \right) \quad (4b)$$

We introduce the center of mass velocity \mathbf{C} and a separation velocity \mathbf{S} :

$$\mathbf{C} = \phi \mathbf{v}_f + (1-\phi) \mathbf{v}_m \quad (5a)$$

$$\mathbf{S} = \phi(\mathbf{v}_f - \mathbf{v}_m) \quad (5b)$$

We further assume that the center of mass velocity \mathbf{C} is zero.

These assumptions are consistent with both following statements: (1) the convective flow and the diapiric flow driven by the buoyancy of the mush have characteristic wavelengths much larger than that of compaction; (2) the reference frame for the computation moves with the convective and diapiric flows. In Section 4 we show that these hypotheses are reasonable to model carbonatitic

Table 1
Characteristics of the magmons generated in the LVZ

	Mantle type	N	Size (km)	Velocity (cm/yr)	Maturation time (My)
Carbonatitic melts	Normal	3	1	9	3
		2	3	60	1
	Hot	3	0.3	9	1
		2	1	60	0.3
High alkaline mafic silicate melts	Normal	3	0.3	0.8	7.5
		2	0.5	2	5
	Hot	3	0.1	0.8	2.5
		2	0.15	2	1.5

This table gives an estimation of the wave-train velocity at the initiation of the compaction process, on the size of the generated magmon and the time for the generation of a mature magmon. The wave initial velocity is $\approx nS^{\text{sc}}/\phi_0$, the size of the magmon is $\approx L$, and the maturation time is $100T^{\text{sc}}$, respectively (see Eqs. 9a–d and 10a–d and Section 4). These quantities depend on the power law coefficient n relating permeability to melt concentration (Eq. 1); on the mantle viscosity μ_m and permeability $k(\phi)$ ($\mu_m \approx 10^{18} \text{ Pa s}$ or 10^{19} Pa s in hot and normal type of mantle, $k(\phi) \sim 10^{-15} \text{ m}^2$ when $\phi \sim 0.01$), and on the melt viscosity μ_f and melting rate ϕ_0 ($\approx 0.01 \text{ Pa s}$ and 0.1% or 1 Pa and 0.3% for carbonatitic and high alkaline mafic silicate melt, respectively): see Section 1 and Section 5.

and high alkaline mafic melt percolation in the mantle. These simplifications lead to following set of equations:

$$\frac{\partial \phi}{\partial t} = -\vec{\nabla} \cdot ((1-\phi)\mathbf{S}) \quad (6a)$$

$$\frac{\mu_f}{k(\phi)}\mathbf{S} = -\vec{\nabla} P' + \Delta P \vec{\nabla} \phi \quad (6b)$$

$$\begin{aligned} \vec{\nabla} \cdot \left((1-\phi) \frac{4\mu_m}{3} \vec{\nabla} \mathbf{S} \right) - \frac{\mu_f}{k(\phi)} \mathbf{S} = \\ - (1-\phi) (\delta \rho g z + \vec{\nabla} \cdot (\Delta P)) \end{aligned} \quad (6c)$$

where $P' = P_f + \rho_f g z$ designates the effective melt pressure. We now consider the case of an infinitesimal melt concentration ϕ , i.e. that $(1-\phi) \approx 1$. Then using Eqs. 2a,b, 5a,b and 6a, we find that:

$$\Delta P = \frac{\mu_m}{\phi} \vec{\nabla} \cdot \mathbf{S} \quad (7a)$$

$$\frac{\partial \phi}{\partial t} = -\nabla \cdot \mathbf{S} \quad (7b)$$

$$\mathbf{S} = \frac{k(\phi)}{\mu_f} \left(-\vec{\nabla} P' + \frac{\mu_m}{\phi} \vec{\nabla} \cdot \mathbf{S} \vec{\nabla} \phi \right) \quad (7c)$$

$$\frac{k(\phi)}{\mu_f} \vec{\nabla} \cdot \left(\frac{\mu_m}{\phi} \vec{\nabla} \cdot \mathbf{S} \right) - \mathbf{S} = \frac{k(\phi)}{\mu_f} \delta \rho g z \quad (7d)$$

The divergence of the Darcy and plastic equations (Eqs. 7c and 7d) and Eq. 7a leads to the following final set of equations:

$$\frac{\partial \phi}{\partial t} = -\frac{\phi \Delta P}{\mu_m} \quad (8a)$$

$$\frac{\mu_f}{k(\phi)} \mathbf{S} = -\vec{\nabla} P' + \Delta P \vec{\nabla} \phi \quad (8b)$$

$$\vec{\nabla} \cdot \left(\frac{k(\phi)}{\mu_f} \vec{\nabla} \Delta P \right) - \frac{\phi}{\mu_m} \Delta P = \frac{\delta \rho g}{\mu_f} \frac{\partial k(\phi)}{\partial z} \quad (8c)$$

$$\vec{\nabla} \cdot (k(\phi) \vec{\nabla} P') = -\mu_f \frac{\phi \Delta P}{\mu_m} + \vec{\nabla} \cdot (k(\phi) \Delta P \vec{\nabla} \phi) \quad (8d)$$

Note that the 3-D compaction flow depends only on two non-linearly coupled scalar variables: the melt concentration ϕ and the pressure step between solid and melt ΔP .

2.2. Dimensionless equations

In the present study we assume that the solid matrix μ_m and melt μ_f viscosities are uniform. As usual the equations are made dimensionless. We adopt ϕ_0 as unit of melt concentration. The unit of length is the compaction length L :

$$L = \sqrt{\frac{\mu_m k(\phi_0)}{\phi_0 \mu_f}} \quad (9a)$$

The unit of velocity S^{sc} corresponds to the ‘Darcy’ velocity of the melt:

$$S^{\text{sc}} = \frac{\delta \rho g k(\phi_0)}{\mu_f} \quad (9b)$$

The time scale T^{sc} is:

$$T^{\text{sc}} = \frac{L \phi_0}{S^{\text{sc}}} \quad (9c)$$

and accordingly the pressure scale P^{sc} is:

$$P^{\text{sc}} = \frac{\delta \rho g k(\phi_0) \mu_m}{\mu_f L \phi_0} \quad (9d)$$

Then, the dimensionless equations for compaction in a mantle with an infinitesimal melt concentration are:

$$\frac{\partial \phi}{\partial t} = -\phi \Delta P \quad (10a)$$

$$\frac{S}{k(\phi)} = -\vec{\nabla} P' + \Delta P \vec{\nabla} \phi \quad (10b)$$

$$\vec{\nabla}(k(\phi) \vec{\nabla} \Delta P) - \phi \Delta P = \frac{\partial k(\phi)}{\partial z} \quad (10c)$$

$$\vec{\nabla}(k(\phi) \vec{\nabla} P') = -\phi \Delta P + \vec{\nabla}(k(\phi) \Delta P \vec{\nabla} \phi) \quad (10d)$$

This set of equations is the same as the one derived by Scott and Stevenson [23]. It confirms the claim of these authors that the pressure step between the solid and the liquid fractions ΔP can be taken into account in the modeling of the compaction process assuming a $1/\phi$ dependent viscosity law for the solid fraction of the mush. Vasilyev et al. [31] derived compaction equations in viscoelastic rocks with an infinitesimal fluid concentration. Actually, their equations are the same as those derived here provided the elastic deformation terms are set to zero in the equations and the bulk viscosity of the solid is $1/\phi$ dependent.

In the present calculations we assume that the total stress due to the pressure jump between solid and melt $\Delta P \vec{\nabla} \phi$ is distributed as $(1-\phi)\Delta P \vec{\nabla} \phi$ and $\phi \Delta P \vec{\nabla} \phi$ on the solid and the melt phases of the mush, respectively; see Eqs. 3c and 3d. Bercovici and Ricard [32] discussed the possibility that this stress only acts on the solid fraction of the mush when $\mu_r \ll \mu_m$. We verify that both kinds of assumptions lead to the same set of equations provided the melt concentration is infinitesimal. In the above set of equations, if we drop the $1/\phi$ terms due to the pressure jump, we find the compaction equations for an infinitesimal melt concentration derived by McKenzie [18] (see Barcilon and Richter [22]). To conclude, we see that the debate concerning the compaction equations with an infinitesimal melt concentration essentially turns on the existence or not of a pressure jump between solid and fluid in the mush, or equivalently to the behavior of the bulk viscosity with porosity. In the following we compare the solutions of both sets of equations. In order to distinguish them we designate them as constant

bulk viscosity experiments and $1/\phi$ bulk viscosity experiments, respectively.

3. 1-D solitary waves

Let assume a 1-D space, then Eqs. 1 and 7a–d yield:

$$\Delta P = \frac{1}{\phi} \frac{\partial S}{\partial z} \quad (11a)$$

$$\frac{\partial \phi}{\partial t} = -\frac{\partial S}{\partial z} \quad (11b)$$

Also, the integration of Eqs. 9c and 9d yields:

$$\frac{\partial}{\partial z} \left[\frac{1}{\phi} \frac{\partial S}{\partial z} \right] - \frac{S}{\phi^n} = -1 \quad (11c)$$

$$\frac{\partial P'}{\partial z} = -\frac{S}{k(\phi)} + \frac{1}{\phi} \frac{\partial \phi}{\partial z} \frac{\partial S}{\partial z} \quad (11d)$$

Let seek for solitary waves and write:

$$\phi = F(z-ct) \quad (11e)$$

In the above expression c designates the solitary wave velocity and F the solitary wave shape function. In the following, we will look for periodic solutions of Eqs. 11a–e. Amongst the possible solutions, we present two specific cases that may be considered as end-members from their specific shape. One type of solitary waves, studied in Section 3.1, has already been considered by Scott and Stevenson [23]. It displays a bulk flat minima, but steep slope, we called it a ‘witch hat’. The second type, studied in Section 3.2, has never been described. As it displays a flat maximum and a slow growing slope, we call it a ‘bowler hat’.

3.1. Periodic solitary wave with flat minima: ‘witch hat melt compaction waves’

Let us assume that the wave function F has a flat minimum $f_0 > 0$ (i.e. when $F(z) = f_0$, $F'(z) = F''(z) = 0$) and a maximum equal to $f_m > f_0$. In Appendix A1 we derive the equation allowing

the calculation of F . Also in [Appendix A1](#) we show that the solitary wave velocity c verifies:

$$c = f_0^{n-1} \frac{\left(Ln\left(\frac{f_m}{f_0}\right) - \frac{1}{n} \left(1 - \frac{f_0^n}{f_m^n}\right) \right)}{\left(-\frac{1}{n} \left(1 - \frac{f_0^n}{f_m^n}\right) + \frac{1}{n-1} \left(1 - \frac{f_0^{n-1}}{f_m^{n-1}}\right) \right)} \quad (12)$$

For instance, if f_0 is small in comparison with f_m :

$$c \approx n(n-1)f_0^{n-1} Ln\left(\frac{f_m}{f_0}\right) \quad (13)$$

Let us assume that the solitary wave has a small amplitude and propagates in a constant porosity medium. Hence, we can write that $f_0 = 1$, and $f_m = 1 + \varepsilon$, where ε is a small quantity. Then a second order approximation of [Eq. 12](#) yields:

$$c \approx n \quad (14)$$

This is the well-known velocity of solitary waves whether there is or not a pressure step ΔP between melt and solid [\[22,23\]](#). It indicates that the pressure step ΔP has a weak effect on the velocity of the solitary wave provided the maximum and minimum of this wave are close. [Eq. 12](#) indicates that the velocity of the solitary wave is a decreasing function of f_0 . Moreover, if the maximum amplitude of the wave f_m remains bounded, its velocity tends to zero when its minimum f_0 tends to zero. It means that the solitary wave cannot cross a domain of zero porosity.

[Fig. 1a](#) shows the melt concentration shape F of several solitary waves. These profiles are finite difference solutions of the differential [Eq. A1.4](#) of [Appendix A1](#) when $f_m = 1$ and $n = 3$. Note that the length of the wave strongly decreases with f_0 . When f_m/f_0 exceeds 2, the wavelength of the solitary wave is several times the-compaction length L . Because of the sharpness of the maxima of this type of wave we propose to call them ‘witch hat melt compaction waves’.

3.2. Periodic solitary wave with flat maxima: ‘bowler hat melt compaction waves’

Here we assume that the maximum of the wave

f_m is flat, i.e. that when $F(z) = f_m$, $F'(z) = F''(z) = 0$. In [Appendix A2](#) we show that the solitary wave velocity c verifies:

$$c \geq n f_m^{n-1} \quad (15)$$

[Fig. 1b](#) shows the wave function F when the velocity of the solitary wave c is 3.2 and 4, and when $n = 3$ and $f_m = 1$. As prescribed by the initial conditions, the top of the waves is flat. Their minima are equal to zero. These minima are discontinuous points for F' . In fact, the curves turn back when $F = 0$, i.e. $F' = \pm \infty$ at both sides of these points. The wavelength of the waves is a few times $10L$ and is seen to decrease with an increasing wave velocity c ([Fig. 1b](#)). Comparison of [Fig. 1a](#) and [Fig. 1b](#) shows that the wavelength of the periodic solitary waves is larger when the top of the wave is flat than when the bottom is flat. For instance, the wavelength of the periodic wave with flat maxima and a dispersion velocity $c = 3.2$ (see [Eq. 15](#)) is about $40L$ instead of a few times L when the minima are flat. Because of the flatness of the maxima of this type of wave we propose to call them ‘bowler hat melt compaction waves’.

The solitary waves described above are only one example among a large variety of similar ‘bowler hat solitary waves’. For instance, instead of assuming that the melt shape function F is flat at its maximum, we can prescribe its curvature $(\partial^2 F / \partial z^2) = f''_m$ at these same points. In [Appendix A3](#) we show that the dispersion relation of this type of wave is:

$$c \geq \frac{f_m^{n-1}}{(1 - f''_m / f_m^{n-2})} \quad (16)$$

This expression proves that if the concavity of the solitary wave at its top f''_m is non-zero, the velocity c of the solitary wave strongly decreases. In [Fig. 1b](#) we display the shape function F when: $f_m = 1$, $f''_m = -1$, $c = 0.7$ and $n = 3$. The profile shows that the non-flatness of the top of the waves is associated with a strong reduction of the solitary wave wavelength. The minimum of the wave function F is also zero and corresponds to a discontinuity of F' .

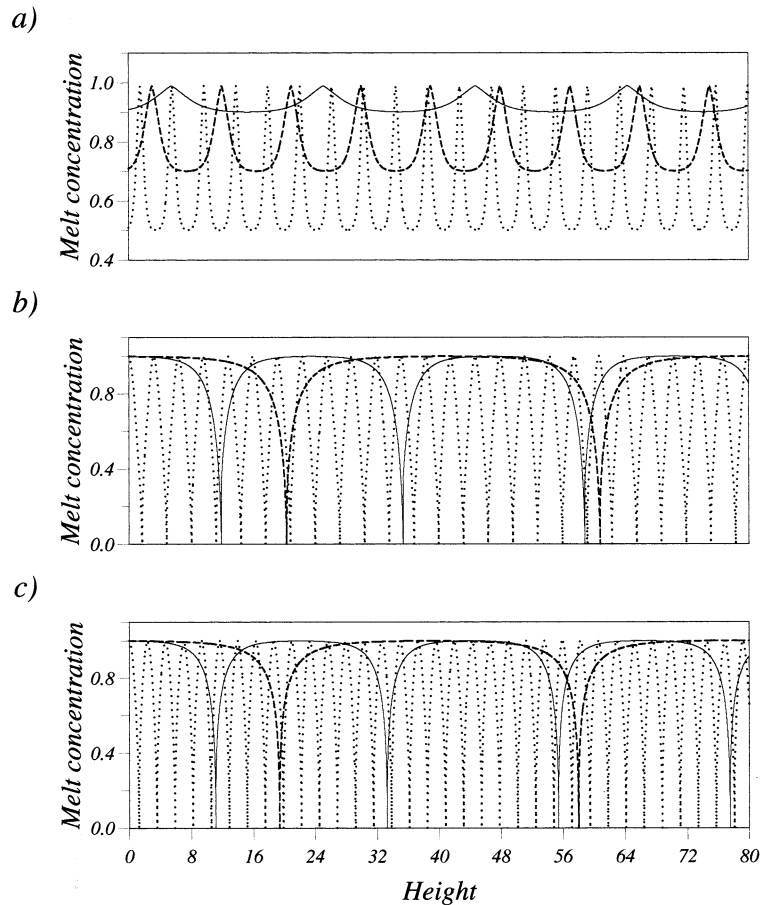


Fig. 1. Melt concentration vs. height of periodic solitary waves. A cubic relationship between permeability and melt concentration is assumed ($n=3$ in Eq. 1), and the maximum amplitude of the wave function $f_m=1$. An $1/\phi$ bulk viscosity is used to compute the profiles in (a) and (b), and a constant bulk viscosity is used for those in (c). (a) displays solitary waves with flat minima designed as ‘which hat waves’. The minimum of the wave function f_0 is 0.8, 0.5 and 0.3, respectively. (b) and (c) display solitary waves with flat maxima designed as ‘bowler hat waves’. The plain line and dashed line waves have a curvature at their maxima $f''_m=0$; the pointed line wave has a curvature $f''_m=-1$. The velocity c of the dashed line wave is 3.2, the one of the plain line wave is 4, and that of the pointed line is 0.7.

The bowler hat waves also happen when the solid and the liquid pressures are assumed to be equal ($\Delta P=0$), i.e. when we look for solitary wave solutions of the constant bulk viscosity compaction equations. In Appendix A4 we show that the dispersion relation of the wave when $f''_m \leq 0$ verifies:

$$c \geq \frac{f_m^{n-1}}{(1-f''_m f_m^{n-1})} \quad (17)$$

Fig. 1c shows the shape functions F corresponding to such type of solitary waves in the case where $n=3$. Their wavelengths are very similar to those taking into account of the pressure jump ΔP . Comparison of Eqs. 16 and 17 indicates that the pressure jump increases the velocity of the solitary waves. This unexpected result is justified by the amplification of the pressure gradients near the minima of the solitary waves due to ΔP (see Eq. 7a).

4. 1-D transient evolution of compaction waves

Because of non-linearity of the compaction equations only some of the solitary waves considered above can grow. In fact, the nature develops those which are stable solutions of the transient non-linear equations (Eqs. 11a–e). Studying the stability of a solution requires relatively heavy mathematical developments. Hence, in order to observe which type of solitary wave is selected by nature, we find it easier to develop 1-D explicit transient numerical simulations of compaction. To generate transient waves, a necessary and sufficient condition is to start the experiment with a concentration profile decreasing upward [24]. Therefore we initiate the experiments with the following melt concentration profile F_{in} :

$$F_{in}(z) = 1 \text{ if } z \leq 25 \tag{18a}$$

otherwise:

$$F(z) = \frac{(1-c^\infty)}{\cosh(0.5(z-25))} + c^\infty \tag{18b}$$

In the above expression c^∞ , the asymptotic concentration at $z = +\infty$ is a free parameter. The initial profiles used are drawn in Figs. 2 and 3. The equations are solved with the second order in time and fourth order in space finite difference scheme proposed by Barcion and Richter [22]. We use 4000 grid points in space and 50 000 time steps. We check the stability of the resolution by comparing solutions with a 10 times finer meshing in both time and space [26].

Fig. 2 shows the melt distribution at time 50 for different transient 1-D experiments of compaction. We assume a cubic relationship between permeability and melt concentration; this is equivalent to set $n=3$ in Eq. 1. In Fig. 2, we compare solutions with constant bulk viscosity and solutions with $1/\phi$ bulk viscosity. The evolution of the waves is dramatically dependent on the asymptotic melt concentration of the initial profile c^∞ . When $c^\infty = 0.5$, Fig. 2a, the evolution and shape of the generated wave-train are similar whether constant bulk viscosity or $1/\phi$ bulk viscosity are used: the waves are quasi-sinusoidal and move at a velocity of about 2. Note that a

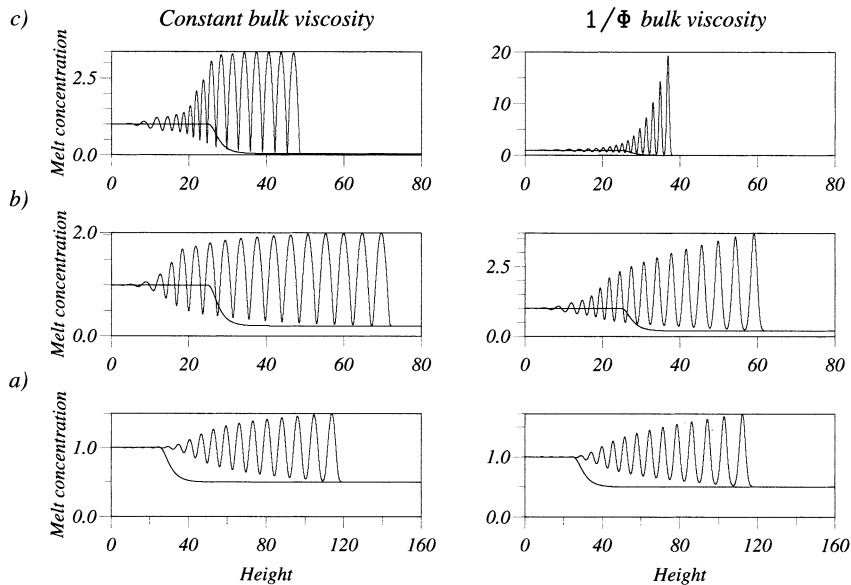


Fig. 2. Comparison of the transient evolution of the waves when the equations are resolved using a constant bulk viscosity and an $1/\phi$ bulk viscosity, respectively. A cubic relationship between permeability and melt concentration is assumed ($n=3$ in Eq. 1). The time $t=50$ snapshot of the melt concentration for three distinct experiments are displayed. The initial melt concentration profiles are also drawn. The cases presented in (a), (b) and (c) differ by the asymptotic melt concentration of the initial profiles c^∞ . It is equal to 0.5, 0.2 and 0.05 in (a), (b) and (c), respectively.

wave velocity $c = 3$ is expected when c^∞ is close to 1 (see Eqs. 14 and 15). The waves reach a dimensionless amplitude of about 1.5. We observe subtle differences in shape between solutions obtained with constant bulk viscosity and $1/\phi$ bulk viscosity, respectively. In particular, the maximum of the wave-train is larger when the bulk viscosity is $1/\phi$ -dependent. The situation when $c^\infty = 0.2$ is displayed in Fig. 2a. The minimum melt concentration in each individual wavelet is buffered by the asymptotic minimum c^∞ . The shape of the two types of wave-trains differs significantly. The constant bulk viscosity waves have acute minima and flat maxima. The $1/\phi$ bulk viscosity wave-train has relatively flat minima and acute maxima. The maxima have amplitudes greater than those found with constant bulk viscosity (3.5 instead of 2). Also, a constant bulk viscosity type wave-train presents a greater velocity than a $1/\phi$ bulk viscosity one (1 instead of 0.7). When $c^\infty = 0.05$, Fig. 2c, no more doubt is permitted: the wave-train generated with constant bulk viscosity belongs to the ‘bowler hat’ family and the

one with $1/\phi$ bulk viscosity to the ‘witch hat’ family. Moreover, the wave-trains have drastic differences in amplitude: 3 compared to 20. Initially, both wave-trains move at a velocity close to 3, i.e. the velocity of solitary waves with small amplitudes (see Eqs. 14 and 15). At time 50, the top of the constant bulk viscosity wave-train has a velocity of 0.4 and a minimum melt concentration equals to c^∞ . With a maximum around $f_m = 3$ and a curvature close to $f''_m = -3$, the velocity of 0.4 is close to the dispersion velocity predicted for constant bulk viscosity bowler-hat solitary wave ($c = 0.3$ according to Eq. 16). The velocity estimate of $1/\phi$ bulk viscosity witch-hat solitary waves depends on both the maximum f_m and the minimum f_0 of the wave function (Eq. 13). At the end of the transient experiment, $1/\phi$ bulk viscosity wave-train verifies: $f_m \approx 20$ and $f_0 = c^\infty = 0.05$. With these parameter values, a dispersion velocity $c = 0.09$ is predicted (Eq. 13), very close to the wave-train velocity of 0.1 measured at the end of the experiment. The good agreement between the velocities recorded in the numerical experi-

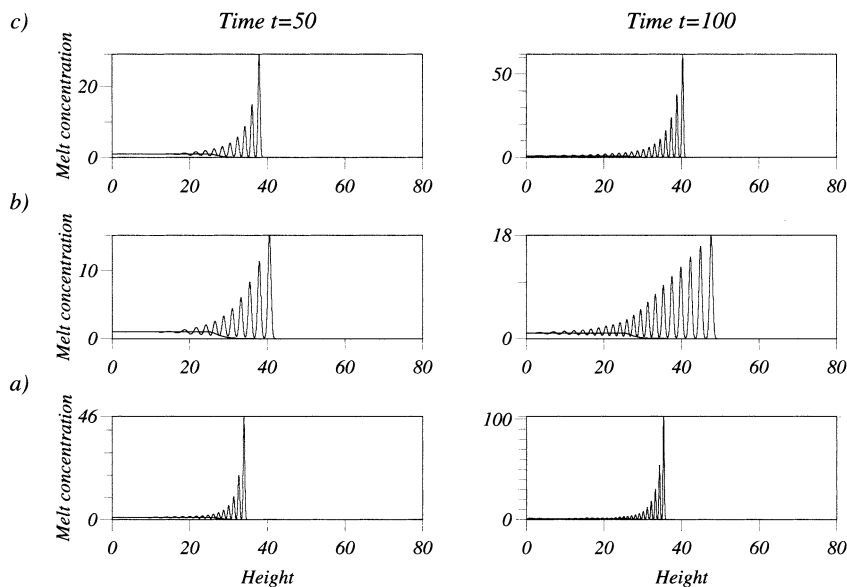


Fig. 3. Comparison of the transient evolution of the compaction waves when the relationship between permeability is cubic ($n=3$) and square ($n=2$). An $1/\phi$ bulk viscosity is used. (a) displays a case with $n=3$, while $n=2$ in the cases shown in (b) and (c), respectively. The cases differ also by the asymptotic melt concentration of the initial profiles c^∞ : $c^\infty = 0.01$ in the case shown in (a) and (b), respectively; $c^\infty = 0.001$ in the case of (c). The time $t = 50$ and time $t = 100$ snapshots of the wave-trains as well as the initial melt concentration profile are drawn.

ments and those deduced from the dispersion relations is striking. It indicates that the periodic solitary waves computed in Section 3 are good approximations of the asymptotic solutions of the transient problem.

In Fig. 3, we compare the evolutions of the wave-trains at time $t=50$ and $t=100$, when the relationship between permeability and melt concentration is cubic ($n=3$) and square ($n=2$). All the experiments are run with an $1/\phi$ bulk viscosity. In the experiments of Fig. 3a,b, the asymptotic concentration of the initial profile $c^\infty=0.01$. Between time 50 and 100, the wave amplitude increases from 46 up to 100 when $n=3$ (Fig. 3a) and from 16 up to 18 when $n=2$ (Fig. 3b). The wave velocity c is extremely small when $n=3$ in agreement with Eq. 14 that predicts $c=0.0055$. When $n=2$, the wave-train moves much faster: in Fig. 3b the wave velocity, at $t=50$, is about 0.14, i.e. close to the prediction of Eq. 13 that is 0.15. In Fig. 3c, we display the $t=50$ and $t=100$ snapshots of an experiment run with $n=2$ and a very small asymptotic melt concentration ($c^\infty=0.001$). In this case, the wave-train reaches a large amplitude: about 62 at $t=100$. We conclude that when the asymptotic concentration c^∞ is very small, the drastic growth of the amplitude of the wave results from the being quasi-motionless of the wave-train when it reaches its asymptotic minimum. This result is independent of the permeability vs. melt concentration law used.

5. Summary and application of the modeling results to mantle metasomatism

We see that the pressure jump ΔP between the solid and melt plays a small effect during compaction provided the initial melt distribution is quite homogeneous. In this case, the compaction waves display a sinusoidal shape and the melt concentration is locally amplified by a factor less than 2. Thus, impregnations with a strong melt concentration cannot be generated. A drastic obstruction at the top of the wetted domain changes the compaction process. Neglecting the pressure jump between solid and melt ΔP , the wave-train has a ‘bowler hat shape’. It crosses domains of zero

permeability (Eq. 17) and locally amplifies the melt concentration by a factor less than 5. Alternatively, the wave-train has a ‘witch hat shape’ and collects a large quantity of melt promoting the development of magmons with a local melt concentration exceeding 100 times the background melt concentration. We infer that carbonatitic and high alkaline mafic silicate melt impregnations can only develop when there is: (1) a drastic obstruction at the top of the mantle column, and (2) a non-zero pressure jump between solid and melt ΔP . In the following we study the conditions leading to a drastic obstruction at the top of the compaction zone and evaluate the possible dimension of the magmons and the time needed to generate them.

5.1. Conditions leading to a drastic obstruction

The mantle carbonatitic and high alkaline mafic silicate melts are generated at a depth below the surface >80 km [27]. It is suspected, while not proved, that the domain of low partial melting below plates coincides with the seismic Low Velocity Zone (LVZ) [33]. Accordingly, the domain of carbonatitic and high alkaline melting extends itself between 200 and 100 km depth. Gradients of temperature inside the convective boundary layer at the base of the lithosphere can be evoked to promote crystallization of this melt and thus induced an upward decrease in melt concentration. This hypothesis is unlikely in case of carbonatitic melts because they are known to crystallize at very low temperatures [34]. More likely, a chemical death of carbonatitic and high alkaline mafic silicate melts results from their interaction with the peridotitic mantle during upwelling [9,10]. Such a process dramatically reduces the relative volume of melt in places where the melt concentration is already low and has a negligible effect in places where it is already high. So, the melt interaction with the peridotites is expected to dramatically decrease the bulk concentration of melt ϕ_0 but has no impact inside the impregnated domains.

The carbonatites and the high alkaline mafic silicate melts are known to be very mobile [9,17]. The carbonatitic melts have a specially

low viscosity: $\mu_f = 0.01\text{--}0.1$ Pa s at temperatures $> 500^\circ\text{C}$ [35–38]. In the following, we assume that $\mu_f = 0.01$ Pa s. The high alkaline mafic silicate melts have a slightly higher viscosity: $\mu_f \approx 1$ Pa s [39]. Nevertheless, as suggested by Hess [16], when the films of fluid are few tens of nanometer thick, the effective viscosity of the melt forming these films is high: in fact it is likely six orders of magnitude greater than normal. We have shown in Section 1 that a few tens of nanometer thick interconnected network of carbonatitic films wrapping the peridotites grains still persists below a melt concentration ϕ of a few 10^{-5} . Hence, when the stiffening of the intergranular melt films occurs, the viscosity jump induces a drastic obstruction to the upward melt percolation. In fact, this obstruction is equivalent to a drop of two and three orders of magnitude in melt concentration ϕ provided the permeability versus melt concentration relationship is cubic or square, respectively [26]. These results indicate that the drastic obstruction necessary to generate magmons with a strong melt concentration must be attributed both to the reduction of melt concentration ϕ resulting from its interaction with the peridotites and to the jump of the interstitial films viscosity below a few tens of nanometer thickness.

5.2. Dimension of the magmons

The magmons have a height about equal to the compaction length L (see Fig. 3). It results that their size depends on the plastic viscosity of the mantle μ_m , the melt viscosity μ_f , and the bulk melting rate ϕ_0 (see Eq. 9a). Rebound data and modeling of mantle convection suggest that the mean plastic viscosity of the LVZ μ_m is of order 10^{19} Pa s [40]. Because of lateral variations of temperature due to mantle convection, lateral variation of viscosity are expected. For instance, an order of magnitude drop in viscosity is likely inside hot plumes: $\mu_m \approx 10^{18}$ Pa s [41,42]. The melting rates ϕ_0 inside the LVZ are not well known. The melting rate of carbonatites in the mantle ϕ_0 is about 0.1% and the one of alkaline mafic silicates melts is just greater: $\phi_0 \sim 0.3\%$ [11,13]. These estimates of μ_m , μ_f , and ϕ_0 imply that the

size of carbonatitic magmons is about 1 km and the one of alkaline mafic silicate melt magmons is sub-kilometric (Table 1).

5.3. Time needed to generate magmons

The models of Fig. 3 show that the time needed to amplify the melt concentration by two orders of magnitude is about 100 in units of T^{sc} (Eq. 9c). According to above parameter value estimates, the carbonatitic magmons are produced in less than 1 Ma and the mafic magmons in several Ma (Table 1). The softening of plastic viscosity μ_m in a hot environment favors the development of smaller structures on a shorter time scale. A ϕ -square permeability relationship enhances permeability and thus favors a faster development of larger structures (Table 1). In the Earth the magmons are also transported by mantle convection. In order to prevent the collision of immature melt impregnations with the lithosphere, the transport of the magmon from its birth to the lithosphere should take more than 1 Ma. Some plume models show upwelling flow in the axis of a hot spot with velocities lower than 10 cm/yr [41]. According to these models, the transport from 200 to 100 km depth takes more than 1 Ma. Other models display convective velocities inside the heart of hot spots exceeding several 10 cm/yr [43]. Also, in the core of a hot spot the carbonatitic or high alkaline mafic silicate melts can be dissolved in the basaltic melts which are produced at comparable depth. These last two settings can likely prevent the two orders of magnitude enhancement of melt concentration during compaction needed to produce the carbonatitic or high alkaline mafic impregnations. We conclude that the development of mature impregnations in the core of a hot spot is not completely impossible, but probably unlikely. The situation is completely different at some distance from the center of any hot spot. There, the upward component of the convective velocities is much lower than 1 cm/yr. The time needed for the partially molten mantle to rise from 200 up to 100 km depth is much greater than 10 Ma. These rules of thumb indicate that the development of carbonatitic or/and high alkaline mafic silicate melt impregnations inside

LVZ domains located apart from the core of a hot spot is very likely.

As a conclusion, we see that the development of carbonatitic and high alkaline mafic silicate melt impregnations is very likely in the LVZ domain apart from the zones of too fast and too hot upwellings. At the top of the LVZ, the thickening of the diffusive boundary layer progressively inhibits the plastic deformation of the solid fraction of the impregnation and thus stops the compaction process. Hence, the impregnations are progressively sealed in the lithosphere well before the crystallization of the trapped melts starts. Accordingly, the impregnations reaching the top of the LVZ have the best chance to be preserved. The trapped carbonatitic and high alkaline mafic silicate melts can be remobilized during a posterior tectonic process. This can explain the modal metasomatism evidenced in some mantle xenolith suites which requires the reaction of mantle peridotites with a relatively high volume of carbonatitic and high alkaline mafic silicate melt (up to 10%, [9,10]). We may also propose that the formation of highly concentrated magmons and their remobilization can explain the eruption of mantle carbonatites and high alkaline mafic silicate melt in continental (in Africa, [27]) and oceanic settings (Cape Verde, Canaries and Kerguelen islands, [44,45]).

Acknowledgements

This research was supported by INSU–Intérieur de la Terre Programme. Constructive reviews by J.L. Vigneresse and D. Yuen greatly improved the manuscript.

Appendix A1. Wave function when the bottom of the wave is flat

Eqs. 11a–e yield:

$$S = c(F + K) \tag{A1.1}$$

$$\frac{\partial}{\partial z} \left[\frac{F'}{F} \right] - \frac{F + K}{F^n} = -\frac{1}{c} \tag{A1.2}$$

where K is a constant of integration and $F = (\partial F / \partial z)$. When $F(0) = f_0$, $F'(0) = F''(0) = 0$, K verifies:

$$K = -f_0 \left(1 - \frac{f_0^{n-1}}{c} \right) \tag{A1.3}$$

If we multiply Eq. A1.2 by F'/F and integrate the product of equations, we obtain:

$$\frac{1}{2} \left(\frac{F'}{F} \right)^2 = -\frac{1}{(n-1)F^{n-1}} - \frac{K}{nF^n} - \frac{1}{c} \text{Ln}(F) + A \tag{A1.4}$$

where A is a constant of integration. At $z=0$, the left hand side of Eq. A1.4 is zero, it implies that:

$$A = \frac{1}{(n-1)f_0^{n-1}} + \frac{K}{nf_0^n} + \frac{1}{c} \text{Ln}(f_0) \tag{A1.5}$$

The right hand side of Eq. A1.4 must be positive for any values of F greater than f_0 and null at the top of the wave $F = f_m$ where $F' = 0$. These conditions are fulfilled if and only if:

$$c = f_0^{n-1} \frac{\left(\text{Ln} \left(\frac{f_m}{f_0} \right) - \frac{1}{n} \left(1 - \frac{f_0^n}{f_m^n} \right) \right)}{\left(-\frac{1}{n} \left(1 - \frac{f_0^n}{f_m^n} \right) + \frac{1}{n-1} \left(1 - \frac{f_0^{n-1}}{f_m^{n-1}} \right) \right)} \tag{A1.6}$$

Eqs. A1.1 and A1.3 imply that:

$$S = c(F - f_0) + f_0^n \tag{A1.7}$$

The infiltration velocity S is always positive and its maximal velocity is reached at the maximum of the wave. According to Eq. 11d, the effective pressure P' verifies:

$$\frac{\partial P'}{\partial z} = cF \left(\frac{F'}{F} \right)^2 - \frac{1}{F^n} (c(F - f_0) + f_0^n) \tag{A1.8}$$

The first term in the right hand side of Eq. A1.7 is always positive and the last one negative. We have shown above that $(F'/F)^2$ vanishes at the top and the bottom of the wave. Since, $(F - f_0)$ also vanishes at the minima of the wave, we de-

duce that the pressure gradient is -1 at the minima of the wave. At the maxima, the pressure gradient is also negative. These results are consistent with an upward migration of the solitary wave.

Appendix A2. Wave function when the top of the wave is flat

The wave function F is solution of the same differential equation as before provided we change f_0 by f_m (see Eqs. A1.1–A1.5). The resolution of the waveform equation in the $[0, f_m]$ interval is complicated by the singularity of the differential equations Eqs. A1.1–A1.4 at $F=0$, i.e. $(F'/F)^2$ is infinite at $F=0$. To avoid this difficulty we introduce the new variable ψ defined by:

$$\frac{1}{\psi} = \frac{F}{f_m}. \quad (\text{A2.1})$$

Thus Eq. A1.3 becomes:

$$\left(\frac{\psi'}{\psi}\right)^2 = \frac{2}{c} \left[\frac{c}{(n-1)f_m^{n-1}} (1-\psi^{n-1}) + \frac{1}{n} \left(1 - \frac{c}{f_m^{n-1}}\right) (1-\psi^n) + \text{Ln}(\psi) \right] \quad (\text{A2.2})$$

The right hand side of Eq. A2.2 is positive if:

$$c \geq \frac{f_m^{n-1} \left[\frac{1}{n} (\psi^n - 1) - \text{Ln}(\psi) \right]}{\left[\frac{1}{n} (\psi^n - 1) - \frac{1}{n-1} (\psi^{n-1} - 1) \right]} \quad (\text{A2.3})$$

When ψ is just greater than 1, the last inequality yields to Eq. 15. The infiltration velocity S writes:

$$S = cf_m \left(\frac{1}{\psi} - 1 \right) + f_m^n \quad (\text{A2.4})$$

It is a continuous function at the minimum of the wave function F , while S' is discontinuous at these same points. The infiltration velocity S is positive close to the maximum of the F -function: $((1/\psi)=0)$ and negative at their minima $((1/\psi)=-1)$. This means that the melt moves upward at

the maxima of the wave and downward at their minima where the melt concentration is zero. Eq. 11d shows that the pressure gradient is:

$$\frac{\partial P'}{\partial z} = -\frac{\psi^n}{f_m^n} \left(cf_m \left(\frac{1}{\psi} - 1 \right) - f_m^n \right) + \frac{cf_m}{\psi} \left(\frac{\psi'}{\psi} \right)^2 \quad (\text{A2.5})$$

According to Eq. A2.2, the pressure gradient $\partial P'/\partial z$ is negative when $\psi=1$ and equal to $-\infty$ at $\psi=+\infty$. This is consistent with an upward interstitial melt velocity of the solitary wave.

Appendix A3. Wave function when the concavity of the top of the wave is fixed

$F(0)=f_m$, $F'(0)=0$ and $F''(0)=f_m''$. Then the differential equation controlling evolution of the melt concentration is:

$$\left(\frac{\psi'}{\psi}\right)^2 = \frac{2}{cf_m^{n-1}} \left[\frac{c}{(n-1)} (1-\psi^{n-1}) + \frac{1}{n} (f_m^{n-1} - c(1-f_m'' f_m^{n-2})) (1-\psi^n) + f_m^{n-1} \text{Ln}(\psi) \right] \quad (\text{A3.1})$$

leading to the dispersion relation

$$c \geq \frac{f_m^{n-1} \left[\frac{1}{n} (\psi^n - 1) - \text{Ln}(\psi) \right]}{\left[\frac{1}{n} (\psi^n - 1) (1 - f_m'' f_m^{n-2}) - \frac{1}{n-1} (\psi^{n-1} - 1) \right]} \quad (\text{A3.2})$$

Appendix A4. Wave function when the pressure of liquid and the solid is the same

$\Delta P=0$. In this case the $(1/\phi)$ -term in Eq. 11c must be dropped and the equation becomes:

$$\frac{\partial}{\partial z} \left[\frac{\partial S}{\partial z} \right] - \frac{S}{\phi^n} = -1 \quad (\text{A4.1})$$

which yields by integration:

$$\left(\frac{\psi'}{\psi^2}\right)^2 = \frac{2}{cf_m^n} [c((n-2)(1-\psi) + (n-3)\ln(\psi)) + \frac{1}{n-1}(f_m^{n-1} - c(1-f_m'' f_m^{n-1}))(1-\psi^{n-1}) + f_m^{n-1} \left(1 - \frac{1}{\psi}\right)] \quad (\text{A4.2})$$

References

- [1] D. Bercovici, Y. Ricard, G. Schubert, A two phase model for compaction and damage, 1, general theory, *J. Geophys. Res.* 106 (2001) 8887–8906.
- [2] D.H. Green, M.E. Wallace, Mantle metasomatism by ephemeral carbonatite melts, *Nature* 336 (1988) 459–462.
- [3] J.M. Dautria, C. Dupuy, D. Takherist, J. Dostal, Carbonate metasomatism in the lithospheric mantle: Peridotite xenoliths from a mellitic district of the Sahara basin, *Contrib. Mineral. Petrol.* 111 (1992) 37–52.
- [4] W.L. Griffin, J.J. Gurney, C.G. Ryan, Variations in trapping temperatures and trace elements in peridotite-suite inclusions from African diamonds: Evidence for two inclusion suites, and implications for lithosphere stratigraphy, *Contrib. Mineral. Petrol.* 110 (1992) 1–15.
- [5] R.L. Rudnick, W.F. McDonough, B.W. Chappell, Carbonate metasomatism in the northern Tanzanian mantle: Petrographic and geochemical characteristics, *Earth Planet. Sci. Lett.* 114 (1993) 463–475.
- [6] R.J. Sweeney, A.B. Thompson, P. Ulmer, Phase relations of a natural MARID composition and implication for MARID genesis, lithospheric melting and mantle metasomatism, *Contrib. Mineral. Petrol.* 115 (1993) 225–241.
- [7] F. Chalot-Prat, A.M. Boullier, Metasomatism in the subcontinental mantle beneath the Eastern Carpathians (Romania): New evidence from trace element geochemistry, *Contrib. Mineral. Petrol.* 129 (1997) 284–307.
- [8] D.A. Ionov, Trace element composition of mantle-derived carbonates and coexisting phases in peridotite xenoliths from alkali basalts, *J. Petrol.* 39 (1998) 1931–1941.
- [9] G.M. Yaxley, D.H. Green, V. Kamenetsky, Carbonate metasomatism in the southeastern Australian lithosphere, *J. Petrol.* 39 (1998) 1917–1930.
- [10] M. Gregoire, B.M. Moine, S.Y. O'Reilly, J.Y. Cottin, A. Giret, Trace element residence and partitioning in mantle xenoliths metasomatised by high alkaline silicate and carbonate-rich melts (Kerguelen Islands, Indian Ocean), *J. Petrol.* 41 (2000) 477–509.
- [11] P.J. Wyllie, W.L. Huang, Peridotite, kimberlite and carbonatite explained in the system explained in the system CaO–MgO–SiO₂–CO₂, *Geology* 3 (1975) 621–624.
- [12] N.M.S. Rock, Lamprophyres, Blackie, Glasgow, 1991.
- [13] J.A. Dalton, D.C. Presnall, The continuum of primary carbonatitic–kimberlitic melt compositions in equilibrium with lherzolite: Data from the system CaO–MgO–Al₂O₃–SiO₂–CO₂ at 6 GPa, *J. Petrol.* 39 (1998) 1953–1964.
- [14] R.H. Hunter, D. McKenzie, The equilibrium geometry of carbonate melts in rocks of mantle composition, *Earth Planet. Sci. Lett.* 92 (1989) 347–356.
- [15] E.B. Watson, J.M. Brenan, D.R. Baker, Distribution of fluids in the continental lithospheric mantle, in: M.A. Menzies (Ed.), *The Continental Lithospheric Mantle*, Clarendon, Oxford, 1990, pp. 111–125.
- [16] P.C. Hess, Thermodynamics of thin fluid films, *J. Geophys. Res.* 99 (1994) 7219–7229.
- [17] W.G. Minarik, E.B. Watson, Interconnectivity of carbonate melt at low melt fraction, *Earth Planet. Sci. Lett.* 133 (1995) 423–437.
- [18] D. McKenzie, The generation and compaction of partially molten rock, *J. Petrol.* 25 (1984) 713–765.
- [19] S. Maaloe, Å. Scheie, The permeability controlled accumulation of primary magma, *Contrib. Mineral. Petrol.* 81 (1982) 350–357.
- [20] N.H. Sleep, Segregation of magma from a mostly crystalline mush, *Geol. Soc. Am. Bull.* 85 (1978) 1225–1232.
- [21] D.J. Stevenson, Spontaneous small scale melt segregation in partial melts undergoing deformation, *Geophys. Res. Lett.* 16 (1989) 1067–1070.
- [22] V. Barcion, F.M. Richter, Non-linear waves in compacting media, *J. Fluid Mech.* 164 (1986) 429–448.
- [23] D. Scott, D.J. Stevenson, Magma solitons, *Geophys. Res. Lett.* 11 (1984) 1161–1164.
- [24] C. Wiggins, M. Spiegelman, Magma migration and magmatic solitary waves in 3-D, *Geophys. Res. Lett.* 22 (1995) 1289–1292.
- [25] A. Ghods, J. Harkani-Hamed, Melt migration beneath mid-ocean ridges, *Geophys. J. Int.* 140 (2000) 687–697.
- [26] M. Rabinowicz, P. Genthon, G. Ceuleneer, M. Hillairer, Compaction in a mantle mush with high melt concentrations and the generation of magma chambers, *Earth Planet. Sci. Lett.* 188 (2001) 213–327.
- [27] K. Bell, B.A. Kjarsgaard, A. Simonetti, Carbonatites into the twenty-first century, *J. Petrol.* 39 (1998) 1839–1845.
- [28] I.S. Sumita, S. Yoshida, M. Kumazawa, Y. Hamano, A model for sedimentary compaction of a viscous medium and its application to inner core growth, *Geophys. J. Int.* 124 (1996) 502–524.
- [29] Y. Ricard, D. Bercovici, G. Schubert, A two phase model for compaction and damage, 2. Application to compaction, deformation, and the role of interfacial surface tension, *J. Geophys. Res.* 106 (2001) 8907–8924.
- [30] C.B. Agee, D. Walker, Olivine flotation in mantle melt, *Earth Planet. Sci. Lett.* 114 (1993) 315–324.
- [31] O.V. Vasiliev, Y.Y. Podlachikov, D.A. Yuen, Modeling of compaction driven flow in poro-viscoelastic medium using adaptive wavelet collocation method, *Geophys. Res. Lett.* 25 (1998) 3239–3242.

- [32] D. Bercovici, Y. Ricard, Energetics in a two-phases model of lithospheric damage, shear localization and plate boundary formation, *Geophys. J. Int.*, submitted for publication.
- [33] J.W. Schlue, L. Knopoff, Shear wave polarization anisotropy in the Pacific Basin, *Geophys. J. R. Astr. Soc.* 49 (1977) 145–165.
- [34] M.J. Le Bas, Nephelinites and carbonatites, in: J.G. Fitton, B.G.J. Upton (Eds.), *Alkaline Igneous Rocks*, Blackwell, *Geol. Soc. Spec. Publ.* 30, 1989, pp. 53–84.
- [35] J.B. Dawson, H. Pinkerton, G.E. Norton, D.M. Pyle, Physicochemical properties of alkali carbonatite lavas data from the 1988 eruption of Oldoinyo Lengai, Tanzania, *Geology* 18 (1990) 260–263.
- [36] D.P. Dobson, A.P. Jones, R. Rabe, T. Sekine, K. Kurita, T. Taniguchi, T. Kondo, T. Kato, O. Shimomura, S. Urakawa, In-situ measurement of viscosity and density of carbonate melts at high pressure, *Earth Planet. Sci. Lett.* 143 (1996) 207–215.
- [37] W.G. Minarik, Complications to carbonate melt mobility due to the presence of an immiscible silicate melt, *J. Petrol.* 39 (1998) 1965–1973.
- [38] J.A. Wolff, Physical properties of carbonatite magmas inferred from molten salt data, and application to extraction patterns from carbonatite silicate magma chambers, *Geol. Mag.* 131 (1994) 143–153.
- [39] D. McKenzie, The extraction of magma from the crust and mantle, *Earth Planet. Sci. Lett.* 74 (1985) 81–91.
- [40] L.M. Cathles, *The Viscosity of the Earth's Mantle*, Univ. Press, Princeton, 1975.
- [41] N.M. Ribe, U. Christensen, Three dimensional modeling of plume lithosphere interaction, *J. Geophys. Res.* 99 (1994) 669–682.
- [42] M. Monnereau, M. Rabinowicz, E. Arquís, Mechanical erosion and reheating of the lithosphere: a numerical model for hotspot swells, *J. Geophys. Res.* 98 (1993) 809–823.
- [43] G. Ceuleneer, M. Monnereau, M. Rabinowicz, C. Rosemberg, Thermal and petrological consequences of melt migration within mantle plumes, *Phil. Trans. R. Soc. London A* 342 (1993) 53–64.
- [44] B.N. Moine, J.Y. Cottin, S.M.F. Sheppard, M. Gregoire, S.Y. O'Reilly, A. Giret, Incompatible trace element and isotopic (D/H) characteristics of amphibole- and/or phlogopite-bearing ultramafic–mafic xenoliths from Kerguelen islands (TAAF, South Indian Ocean), *Eur. J. Mineral.* 12 (2000) 761–777.
- [45] K. Hoernle, G. Tilton, M.J. Le Bas, S. Duggen, D. Garbe-Schönberg, Geochemistry of oceanic carbonatites compared with continental carbonatites: Mantle recycling of oceanic crustal carbonate, *Contrib. Mineral. Petrol.*, 2002, published online, ref. s004100100308ch100.